

OPTICAL DESIGN OF COMMUNICATION SIMULATOR FOR ORBITAL ANGULAR MOMENTUM  
BASED FREE-SPACE LINK WITH AN ADAPTIVE OPTICS RECEIVER

by

Alonzo Espinoza

---

Copyright © Alonzo Espinoza 2015

A Report Submitted to the Faculty of the

THE COLLEGE OF OPTICAL SCIENCES

In Partial Fulfillment of the Requirements

For the Degree of

MASTER OF SCIENCE  
WITH A MAJOR IN OPTICAL SCIENCES

In the Graduate College

THE UNIVERSITY OF ARIZONA

2015

STATEMENT BY AUTHOR

This report has been submitted in partial fulfillment of requirements for an advanced degree at the University of Arizona and is deposited in the University Library to be made available to borrowers under rules of the Library.

SIGNED: Alonzo Espinoza

APPROVAL BY THESIS DIRECTOR

This report has been approved on the date shown below:

\_\_\_\_\_  
Yuzuru Takashima  
Professor  
The College of Optical Sciences

12/18/2015  
Date

## Contents

Abstract.....	6
1. Introduction .....	7
2. Theory: Orbital Angular Momentum .....	9
3. OAM Generation .....	11
4. Implementation of Test Bed for OAM communications.....	13
5. Pre-Fabrication Simulation .....	16
6. Fabrication of Spiral Phase Plate using Maskless Lithography Tool (MLT) .....	22
7. Simulation Evaluation of Crosstalk .....	28
8. Effects of Defects and Height Error for Experimental Crosstalk.....	32
9. Conclusions and Future Work.....	39
10. Matlab code .....	40
11. References .....	51
List of Publications .....	52

## List of Figures

Figure 1: Intensity patterns for LG equation found in <i>Precision Interferometry in a New Shape</i> . .....	9
Figure 2: Intensity profile of a LG beam with OAM that has increasing center singularity as mode index $l$ increases. ....	10
Figure 3: Different phase profiles of SPP at (a) +1, (b) +2, and (c) +3 mode index.....	11
Figure 4: The combination needed to create a forked hologram. (a) LG beam with stepping phase from $0 \rightarrow 2\pi$ for a +1 mode, white to black gradient respectively (b) blazed plane wave (c) blazed fork hologram .....	12
Figure 5: OAM simulator with AO system [1]. ....	13
Figure 6: Tx and Rx schematics. ....	13
Figure 7: Schematic design of turbulence chamber. ....	15
Figure 8: Transmitter. ....	15
Figure 9: Chamber entrance. ....	15
Figure 10: Receiver.....	15
Figure 12: Output with a new vortex of $l=4$ .....	18
Figure 11: vortex input of $l=3$ .....	18
Figure 14: Output of new vortex with $\alpha=0.9$ . ....	18
Figure 13: Output of vortex with $\alpha=0.2$ . ....	18
Figure 16: Vortex output when $D=-10\%$ . ....	19
Figure 15: Vortex output when $D=+10\%$ .....	19
Figure 17: OAM +1 intensity output with white line. ....	20
Figure 18: OAM +1 intensity output with black line. ....	20
Figure 19: The effects of a black error line on an OAM +3 profile.....	21
Figure 20: MLT block diagram [11]. ....	23

Figure 21: Veeco Measurement of the test mark for height measurement. ....	24
Figure 22: +1 OAM height. ....	25
Figure 23: +2 OAM height. ....	25
Figure 24: +3 OAM height. ....	26
Figure 25: 3D profile of +2 mode. ....	27
Figure 26: 3D profile of +3 mode. ....	27
Figure 27: Simulated output from port 1 and 2 as a function of phase difference between two arms of ideal plane wave sent through the MZ simulator. ....	29
Figure 28: Simulated output from port 1 and 2 as a function of phase difference between two arms of MZ. Ideal OAMs sent through the MZ simulator. ....	30
Figure 29: Simulated output from port 1 and 2 as a function of phase difference between two arms of MZ. Measured OAMs sent through MZ simulator. ....	31
Figure 30: OAM +1 measured and ideal compared side by side. ....	32
Figure 31: OAM +1 difference. ....	32
Figure 32: OAM +2 measured and ideal compared side by side. ....	33
Figure 33: OAM +2 difference. ....	33
Figure 34: Regular beam output seen at each port of actual MZ. ....	34
Figure 35: OAM +1 data. ....	35
Figure 36: OAM +2 data by itself. ....	36
Figure 37: Output of 0 and +1. ....	37
Figure 38: Output of +1 and +2. ....	37

## Abstract

This report addresses fabrication and optical design of components and test bed systems for free-space communications links employing spatial domain multiplexing by using Orbital Angular Momentum (OAM).

Orbital Angular Momentum has been gaining attention in communications systems. The OAM-based and other spatial multiplexing enables to use new degree of freedom independently from constraints such as requirement to have sufficient wavelength spacing for wavelength division multiplexing with high data rate communication channel. The new degree of freedom is spatial mode based multiplexing by using orthogonality of spatial amplitude and phase structure. Therefore, especially for free space communication channel in air, perturbation of the phase front deteriorates orthogonality.

Consequently, the deterioration of the signal causes a decrease in channel capacity. Recently, use of an adaptive optics to compensate for the corrupted phase front is proposed, and its effectiveness is numerically confirmed. For the purpose of experimental demonstration of recovery of phase profile by AO system, a test bed to mimic air turbulence has been developed at the University of Arizona. In these communication system test beds, the OAM mode multiplexing and demultiplexing is crucial functionality. The testbed used involves using a visible monochromatic wavelength as well as a transmitter (Tx) and a receiver (Rx). Specifically, a Spiral Phase Plates (SPP) for OAM creation were designed and lithographically fabricated for multiplexing and demultiplexing. Crosstalk testing through a Mach-Zehnder (MZ) based demultiplexing system is experimentally performed. The experimental results obtained by testbed are compared to a mathematical simulation model to identify possible source of errors to further decrease cross talk. Finally, path way to improve the cross talk performance is suggested as a part of conclusion of the master report.

## 1. Introduction

Free-space based optical links and communications employ Orbital Angular Momentum (OAM) has been getting more attention because of the ability to increase number of spatially multiplex a number of modes, additionally to existing multiplexing methods such as wavelength division multiplexing. The OAM based multiplexing takes advantage of the orthogonality of the OAM modes, which enables to spatially multiplex electromagnetic waves within a common physical transmission channel, for example in air and in fiber. Since the multiplexing process is based on the orthogonal phase profile of the wave front, therefore, it is susceptible aberrations induced by air turbulences. These aberrations increase cross talk with the modes which would potentially inducing limitation on the gain in channel capacity we expect from such spatial multiplexing based communication.

These aberrations are an obstacle with free space communications, but can be mitigated by using adoptive optics (AO) based recovery of the corrupted phase front. It has been found that channel capacity can be recovered by using the AO with sparsely selected OAM modes [1]. As proposed in the paper, the AO and free-space communications have a potential in security and increased data rate and channel capacity. . To verify the feasibility of employing AO with the OAM-based free space communication, a test bed with an air chamber with which artificial air turbulence is created is designed and implemented to quantitatively evaluate how all the components take play in each part of the system.

In the testbed, a transmitter (Tx) will be sending multiplexed OAM modes with modulation of the signal, and the receiver (Rx) will separate the modes to pick up the signals.

The report addresses design fabrication, and testing of a special optical component: a spiral phase plate, which is the major components of the system. Also, report summarizes evaluation result of cross-talk among modes by implementing the SPPs to Tx and Rx, fabrication and experimental evaluation of design.

This report is divided into separate sections to properly overlay the theory and the process for crosstalk evaluation. In Section 2, the mathematical representation of OAM modes is reviewed. In Section 3, the generation of OAM by holograms and SPPs is discussed. In Section 4, the testbed used for crosstalk evaluation is reviewed. In Section 5, the pre-fabrication tests are evaluated and used to compare with actual values from fabrication. In Section 6, the OAM generators are fabricated and the methods used are explained. In Section 7, the MZ simulator is created and tested before applying the measured phase plates. Then in Section 8, the effects of defects in the plates are evaluated using the MZ simulator and is compared to the experimental results. In Section 9, the final section, addresses the future direction of the research based on this report.

## 2. Theory: Orbital Angular Momentum

Electromagnetic fields carry a form of linear momentum a type of external momentum, but depending on the choice of the coordinate system of the electromagnetic wave, there can different solutions with different forms of momentum [2]. A common and the lowest order solution to the wave equation in Cartesian coordinate system is known as the Gaussian beam, but a solution to the same wave equation in the cylindrical coordinates gives us what is known as a Laguerre-Gaussian (LG) beam [3]. Eq. (1) is a form of the LG beam with helical complex amplitude, where  $C_{lp}$  is a normalization constant,  $L_p^{|l|}$  is the Laguerre polynomials,  $r$  is the radial distance from the center axis of the beam, and  $\omega_0$  is the beam waist.

$$\varphi_{l,p}(r, \phi) = \frac{C_{lp}}{\omega_0} \left(\frac{r\sqrt{2}}{\omega_0}\right)^{|l|} L_p^{|l|} \left(\frac{2r^2}{\omega_0^2}\right) \exp\left(-\frac{r^2}{\omega_0^2}\right) \exp(il\phi) \quad (1)$$

The intensity patterns for the helical LG equation can be seen in Fig. 1 [4].

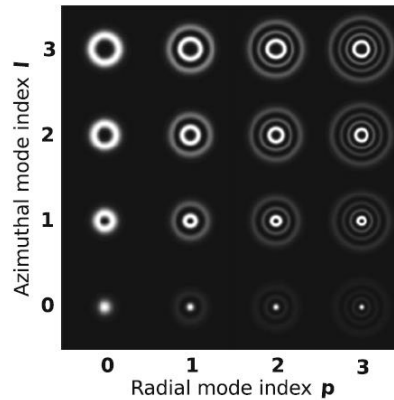


Figure 1: Intensity patterns for LG equation found in *Precision Interferometry in a New Shape*.

The key term that comes from the helical form of the LG equation that produces the OAM in the system is the  $\exp(il\phi)$  term, where  $\phi$  is the azimuthal phase profile taking a value from 0 to  $2\pi$  for one wave, and  $l$  determines the mode which is the number of twists per wavelength. The mode index is an integer,  $l = \pm 1, \pm 2, \pm 3, \dots$ , where it determines the azimuthal phase of the beam. More twists per wavelength the greater singularity of the beam which in turn creates a bigger donut style intensity. Fig. 2 shows a spatial intensity profile of several OAM modes simulated by using a physical optics simulation program OptiScan [5]. As the parameter  $l$  becomes larger (+1, +2, +3), the center of the singularity gets bigger as the number of wavelengths per twist increases which can be seen in Fig. 2.

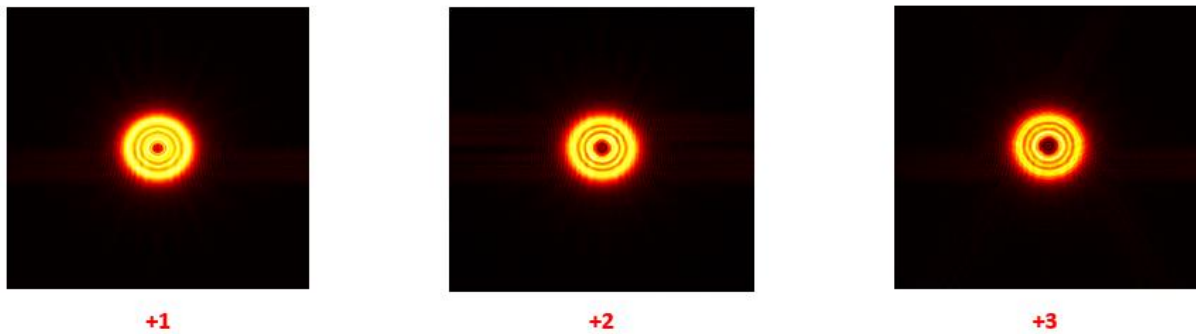


Figure 2: Intensity profile of a LG beam with OAM that has increasing center singularity as mode index  $l$  increases.

### 3. OAM Generation

To create OAM modes a beam shaper to convert Gaussian beam to desired LG models is needed.

Methods of beam shapers include computer generated holograms [6] and spiral phase plates SPP [7].

The beam shapers take a Hermite-Gaussian beam and give the beam a helical structure to recreate it as a LG beam.

A SPP is a direct phase modulation by using a stepping index. The stepping shape gives the input beam a  $0 \rightarrow 2\pi$  phase modulation for one full optical path difference (OPD). A SPP does not have to be a single step, but depending on the mode index the SPP can step multiple times for each full OPD. Thus Fig. 3 shows the phase profile of a SPP at three different modes: +1, +2, and +3.

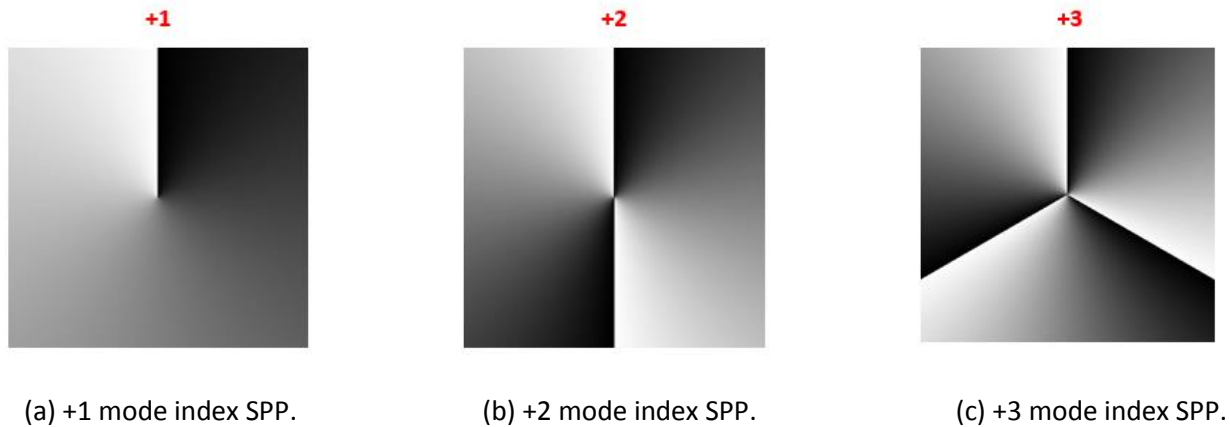


Figure 3: Different phase profiles of SPP at (a) +1, (b) +2, and (c) +3 mode index.

Since the SPP needs to have a stepping index to match the input beam the SPP equation is dependent on Eq. 2 where  $\theta$  represents the azimuthal phase of the SPP,  $\lambda$  is the wavelength,  $l$  is the OAM mode integer, and  $n$  is the index of refraction for the substrate.

$$\frac{\theta l \lambda (n-1)}{2\pi} \quad (2)$$

Alternatively, a computer generated hologram (CGH) can be used as a beam shaper. The CGH is a diffractive optical element (DOE) that creates OAM is called a fork hologram in part to its fork like shape. The fork like shape comes from taking a LG beam created by the azimuthal phase and interfering it with a plane wave. The interference pattern can then be written or etched on a substrate to create a DOE which can be seen in Fig. 3.

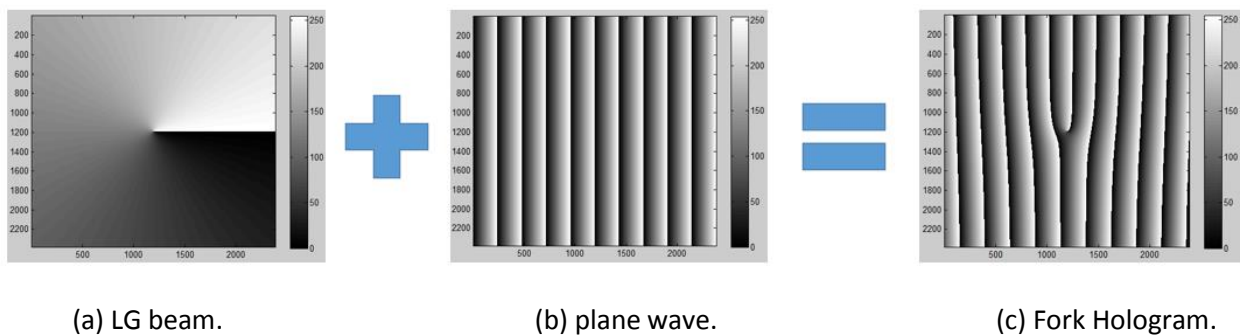


Figure 4: The combination needed to create a forked hologram. (a) LG beam with stepping phase from.  $0 \rightarrow 2\pi$  for a +1 mode, white to black gradient respectively (b) blazed plane wave (c) blazed fork hologram

Fig. 4 in particular shows a LG beam that steps in phase from 0 to  $2\pi$  for a single mode interfering with a blazed pattern that also steps from 0 to  $2\pi$ . This interference creates a blazed fork grating, but a normal binary fork grating can be made as well. The creation of the hologram has a phase modulation given by Eq. (3) where  $\theta$  is the azimuthal phase,  $\lambda$  is the wavelength, and  $l$  is the mode integer. The whole term  $\frac{l\lambda\theta}{2\pi}$  gives the phase profile while  $\alpha x$  gives the binary profile of the hologram.

$$\frac{l\lambda\theta}{2\pi} + \alpha x \quad (3)$$

## 4. Implementation of Test Bed for OAM communications

To understand base-line performance of OAM-based free space communications, Prof. Cvijetic and Prof. Takashima are jointly developing an OAM simulator with AO system depicted in Fig. 5 found in a paper for AO recovery [1].

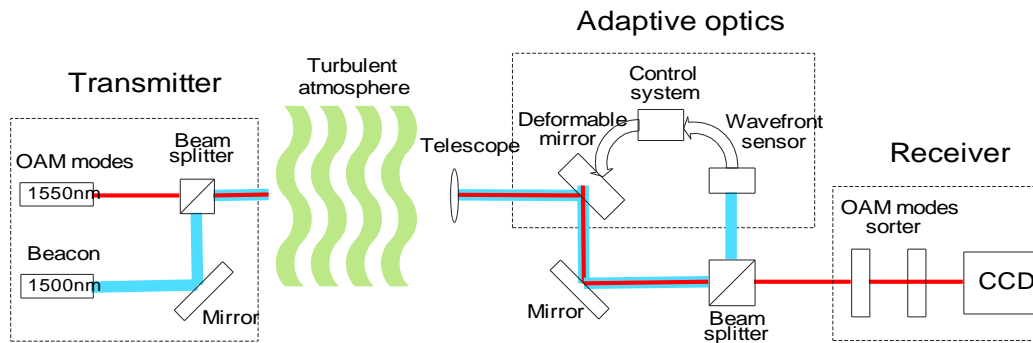


Figure 5: OAM simulator with AO system [1].

The transmitter consists of an input laser, two beam splitters, and two mirrors so that two modes can multiplexed onto each other. Since the OAM modes are multiplexed they will need to be demultiplexed by the receiver which consists of two mirrors, two beam splitters, and two dove prisms. Both the transmitter and receiver can be seen in Fig. 6 with the chamber in between them.

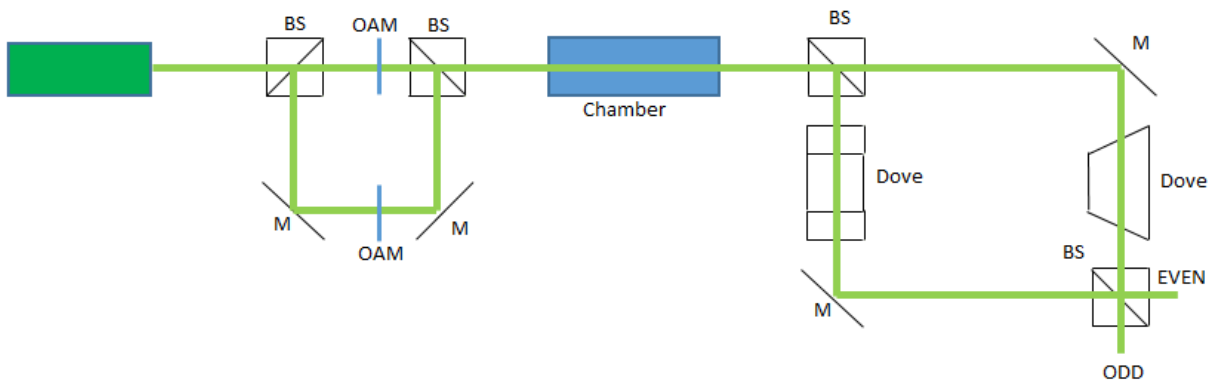


Figure 6: Tx and Rx schematics.

The MZ separator in Fig. 6 is an optical system that separates modes of OAM utilizing the dove prism rotation. OAM modes are orthogonal to each other, for example a +1 and +2 mode are orthogonal, and this can be utilized for OAM separation by rotating phase front of multiplexed beam and interfering them. Gregorius Berkhout showed in his paper that there can be sorting of OAM modes using a spatial light modulator [8]. Jonathon Leach and his group also showed that another method of separation can be done by using a Mach-Zehnder (MZ) interferometer by relying on the  $\exp(il\theta)$  form [9]. The MZ that is used creates an arm path that is rotated given by the angle  $\alpha$  which adds a phase dependence  $\exp(il(\theta + \alpha))$ . This phase rotation is achieved by utilizing dove prisms in each arm path that are rotated at an angle of  $\frac{\alpha}{2}$  with each other. By using different dove prism angles. By introducing an angle of  $\frac{\alpha}{2} = \frac{\pi}{2}$  this gives a phase difference of  $l\pi$ , and by properly setting the path lengths  $l$  can separate pure odd and even modes into separate ports. Then to separate further the modes can cascaded to another MZ with a phase difference of  $\frac{l\pi}{2}$  by making  $\frac{\alpha}{2} = \frac{\pi}{4}$ . This causes modes with a  $l = 4n$  and  $l = 4n + 2$  modes separate, where  $n$  is an integer. The problem with this is that the odd modes cannot be separated the same way because of the fact that they are odd, so before we introduce the same phase difference of  $\frac{l\pi}{2}$ , the odd modes need to undergo an addition of their azimuthal phase by 1. In fact for every cascaded stage of the MZ there needs to be an addition of the azimuthal phase for every stage where odd modes are present, and this can be done using a mode converter.

The turbulence chamber itself in between the Tx and Rx is a cylindrical chamber that will allow perturbation of the signal beam by modulating the air using heating and cooling components as depicted in Fig. 7.

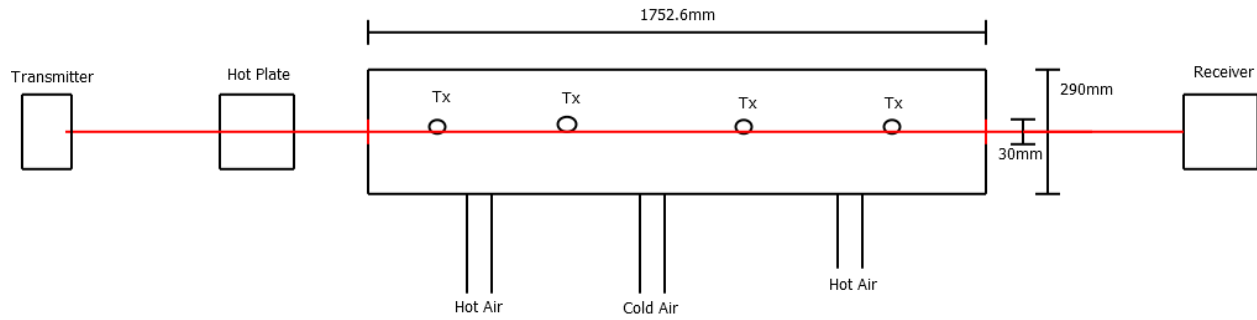


Figure 7: Schematic design of turbulence chamber.

The end goal objectives are to establish a baseline link system, evaluate the effect of air turbulence, and to allow testing of AO compensation. TO ensure a proper link it needs to be seen if crosstalk exists, therefore from the MZ explanation before, two modes of +1 and +2 will be chosen for testing purposes to allow the use of a single MZ.

Fig. 8, 9, and 10 show the Tx, Rx, and chamber.

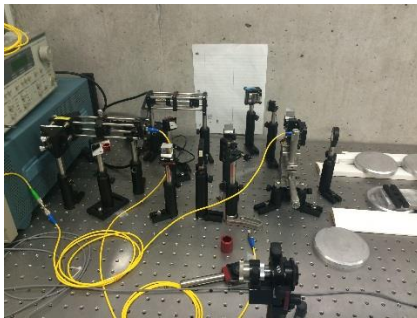


Figure 8: Tx.

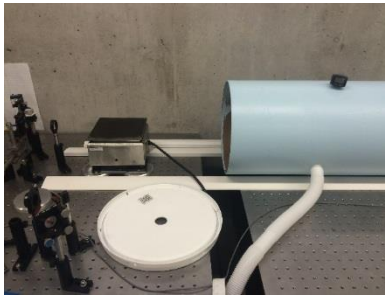


Figure 9: Chamber entrance.

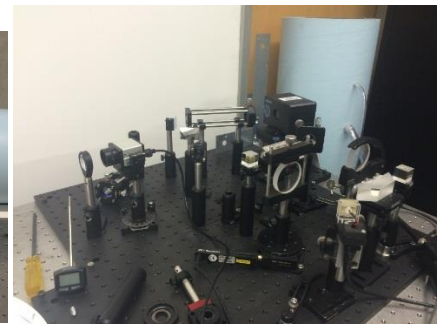


Figure 10: Rx.

## 5. Pre-Fabrication Simulation

The OAM generators can be using a device known as a Maskless Lithography Tool (MLT), which is a freeform exposure on a substrate instead of using the traditional mask etching process from a normal lithography tool [10]. The tool has a linearization process and calibration system for height, so in fabrication there could height errors [11]. Before the SPP is fabricated, there should be a double check the mode conversion process and to simulate possible errors in the phase or missing data from the OAM profiles that can from fabrication using the MLT. Also, in future work with the free space lines, there is an involvement of mode converters for cascaded MZs. Thus there will also simulate a mode converter and test if it will work, and the mode converter will undergo the same errors as the OAM generators as they are also fabricated with the MLT.

A standard optical vortex can be given by Eq. (4) where  $l$  is the charge,  $\phi$  is the azimuthal phase of the (is referred to as  $\theta$  in previous equations),  $k$  is the wavenumber,  $z$  is the direction of propagation,  $\omega$  is the angular frequency, and  $t$  is the time.

$$U^- = \exp[-j(l\phi - kz + \omega t)] \quad (4)$$

The assumed output after mode conversion is given by Eq. (5) where  $\gamma$  is an arbitrary phase given by the mode converter.

$$U^+ = \exp\{-j[(l + \Delta)\phi - kz + \omega t + \gamma]\} \quad (5)$$

This arbitrary phase can be ignored as it will make no difference in the phase profile. The equation of the system can be now represented by Eq. (6), and solving for  $t$  using Eq. (7), (8), and (9) we come to a simplified solution Eq. (10) by introducing a  $\Delta$ .

$$U^+ = tU^- \quad (6)$$

$$t = \frac{U^+}{U^-} = \frac{\exp\{-j[(l+\Delta)\phi - kz + \omega t + \gamma]\}}{\exp[-j(l\phi - kz + \omega t)]} \quad (7)$$

$$t = \exp\{-j[(l + \Delta)\phi - kz + \omega t + \gamma]\} \exp[+j(l\phi - kz + \omega t)] \quad (8)$$

$$t = \exp[-j(l\phi + \Delta\phi - kz + \omega t - l\phi + kz - \omega t - \gamma)] \quad (9)$$

$$t = \exp[-j(\Delta\phi - \gamma)] \quad (10)$$

To simulate possible phase error or total profile error I insert to variables into Eq. (10),  $\alpha$  which will be manipulating everything within the phase, and  $D$  which is directly manipulating the azimuthal phase as a percentage. This new test equation will be given by Eq. (11).

$$t = \exp[-j\alpha(\Delta(D\phi) - \gamma)] \quad (11)$$

For the test the mode converter will be a +1 conversion,  $\Delta = 1$ , and the mode to be  $l = 3$ . First simulation is a perfect mode converter of  $\Delta=1$ ,  $\alpha=1$ , and  $D=1$

Fig. 11 is the input and Fig. 12 is the output.

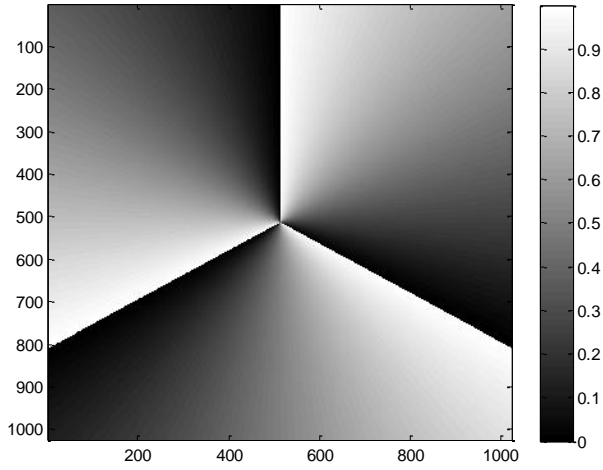


Figure 11: vortex input of  $l=3$ .

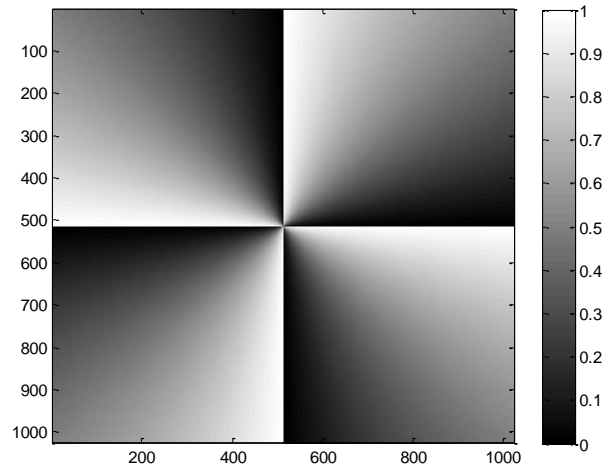


Figure 12: Output with a new vortex of  $l=4$ .

The output is behaving as it should be, now  $\alpha=0.2$  and the output is given as Fig. 13, and finally  $\alpha=0.9$  where the output as Fig. 14.

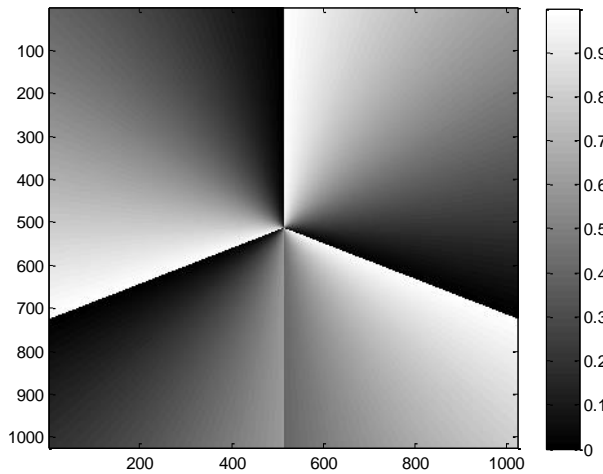


Figure 13: Output of vortex with  $\alpha=0.2$ .

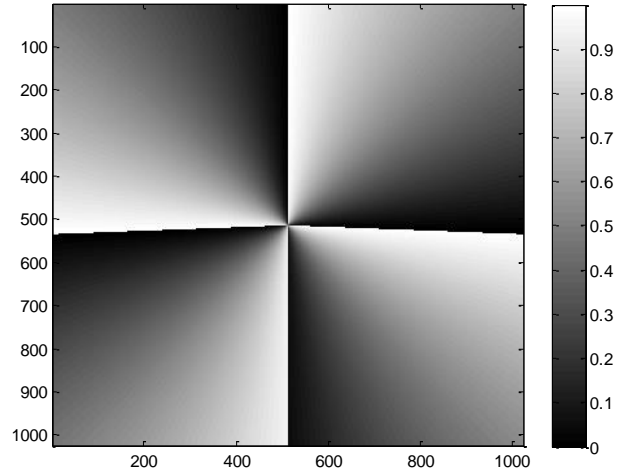


Figure 14: Output of new vortex with  $\alpha=0.9$ .

Next part of simulation testing will involve keeping  $\alpha$  at 1, keeping the input perfect, and changing D to  $\pm 10\%$  of the mode converter. The new outputs, after mode conversion, will be given by Fig. 15 and Fig.

16.

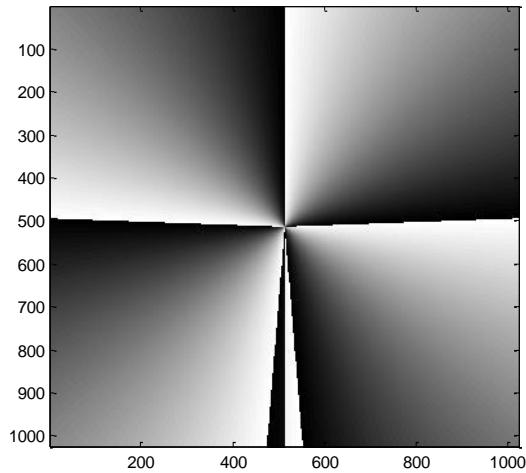


Figure 15: Vortex output when D=+10%.

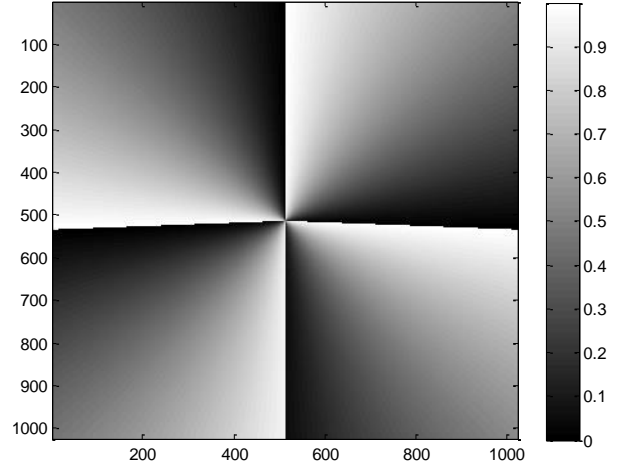


Figure 16: Vortex output when D=-10%.

The  $\alpha$  component had a direct influence on the OAM mode changing and the change of D had a direct change in the phase profile mapping. This shows that an error in the equation can affect all of the phase profile and OAM mode. Another simulation was performed using the software Optiscan to evaluate the intensity output after erasing a line of data from different OAM modes. Using a +1 OAM mode and applying two different lines of pixels which represent black for a full  $2\pi$  and white for zero. Fig. 17 shows how a white line on the phase profile affects the intensity output of the OAM mode, and Fig. 18 shows the intensity output with a black line over the OAM +1 phase profile.

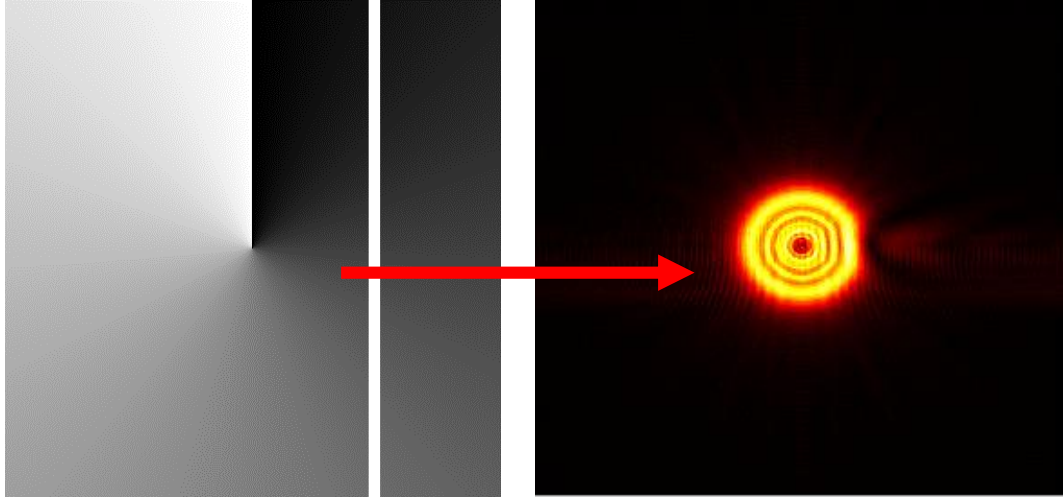


Figure 17: OAM +1 intensity output with white line.

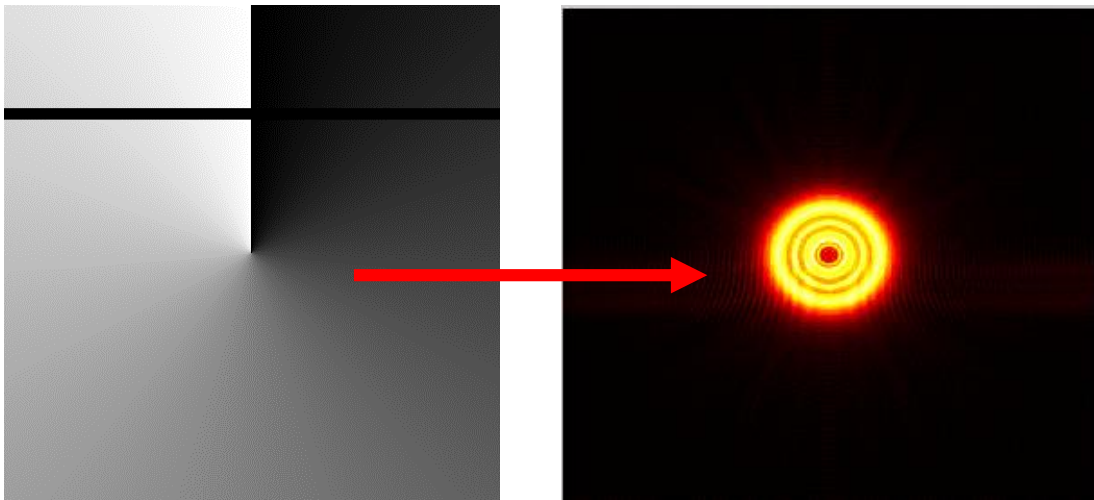


Figure 18: OAM +1 intensity output with black line.

To further see how an error line over the phase profile effects the intensity profile the next test will involve an OAM +3 mode with a black error line through it, which is observed in Fig. 19.

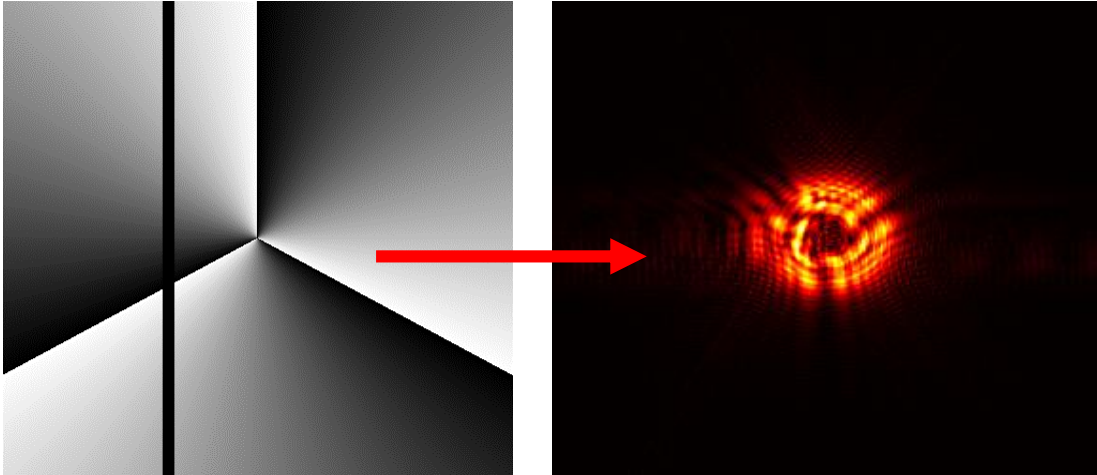


Figure 19: The effects of a black error line on an OAM +3 profile.

From the simulation results shown above it can be assumed that a great detor or corruption of the phase profile can have a negative effect on the donut like intensity. The brightness can go down as compared to Fig. 18 versus Fig. 19 for the OAM +3 intensity, and the overall shape deteriorates.

## **6. Fabrication of Spiral Phase Plate using Maskless Lithography Tool (MLT)**

The MLT will be used to fabricate the OAM generators. The MLT has seven primary components and two major systems seen in Fig. 20 [9]. The first component is the laser source and laser relay that brings it to the optical bench. There are stability optics in the second group to align the laser properly, in the third group there is a beam expander with an acoustic-optic modulator (AOM) to perform modulation, and the fourth part contains anamorphic optics for scanning purposes to coordinate with the fifth part the control software. Finally the scan is sent through the relay optics and to the sample stage where the pattern is etched.

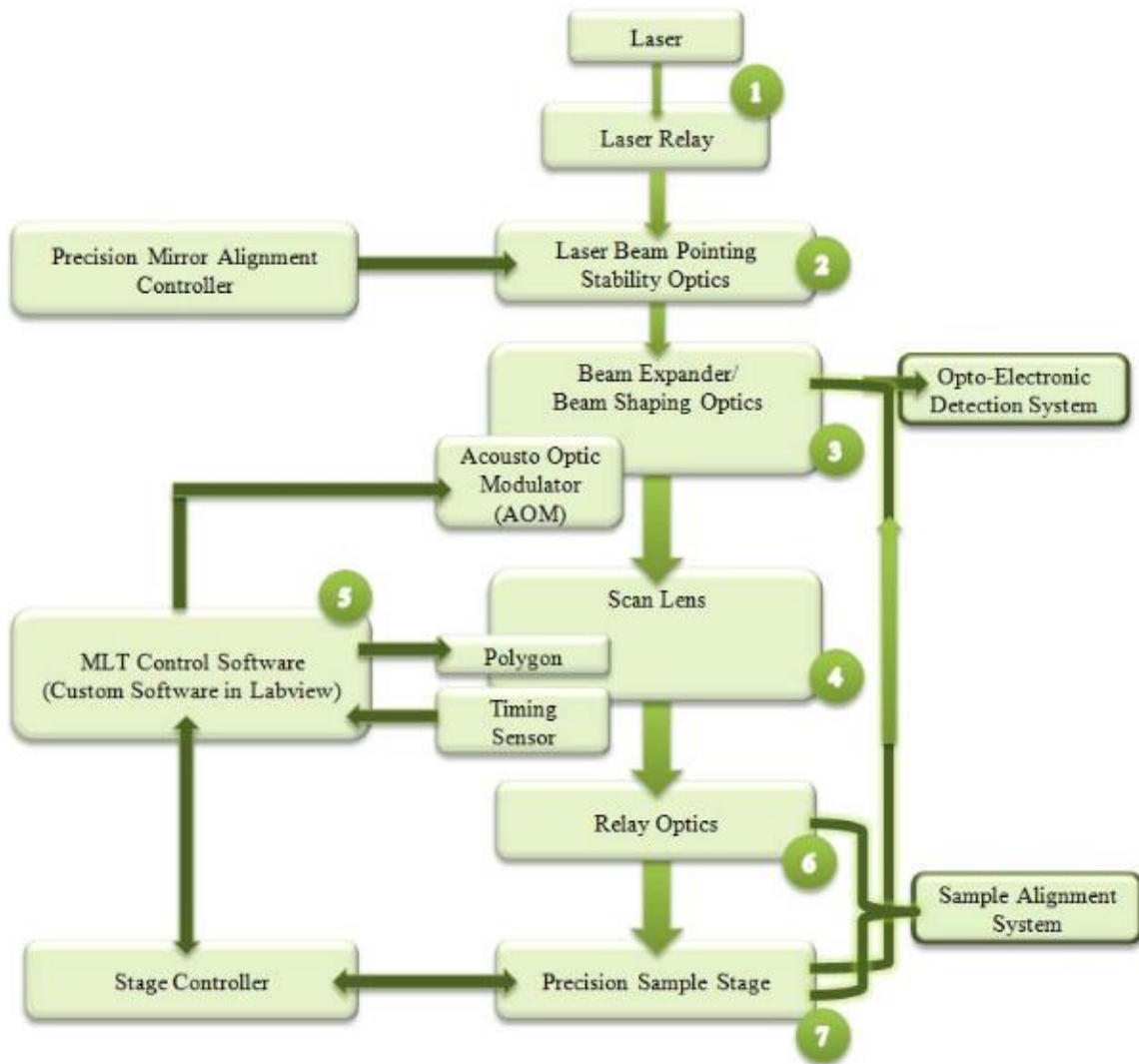


Figure 20: MLT block diagram [11].

The MLT can be used to make a stepping pattern, but since step patterns are difficult to make there could be fabrication errors.

The material that is used Poly10 (Fujifilm, Valhalla, NY) and has a wide coverage of wavelengths for use.

At a wavelength 532nm, the Poly10 has an index of 1.609, and the sample size of creation will be 18mm

by 18mm. Three samples will be made: +1, +2, and +3. Eq. 12 will be able to find the thickness for one full wave of OPD.

$$\frac{\lambda}{n-1} = \frac{.532}{.609} = .8736\mu m \quad (12)$$

Once the height for the material is determined, the mathematically created pattern is uploaded to the MLT. The MLT then goes through a number of passes determined by the MLT parameters, and afterward they are put through a solution to get rid of the excess material. To ensure the height comes out properly a few test marks have been applied on to the SPP patterns. The height of the pattern is measured using a Veeco interferometer. Fig. 21 shows a cross-sectional profile of the test pattern measured by Veeco.

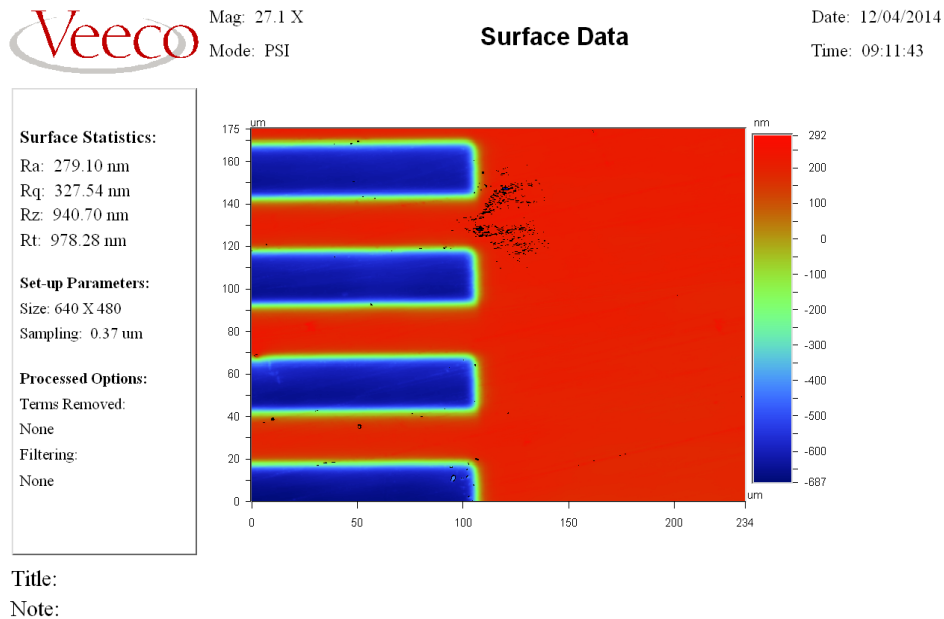


Figure 21: Veeco Measurement of the test mark for height measurement.

After measuring the SPPs the heights obtained are +1 giving  $0.867\mu\text{m}$ , +2 giving  $0.8466\mu\text{m}$ , and +3 giving  $0.8845\mu\text{m}$  height. A  $\pm 5\%$  error in fabrication would be  $\pm 0.04368\mu\text{m}$  which means the height range is  $0.82992\text{--}0.91728\mu\text{m}$ . Fig. 22, 23, and 24 show the Veeco height data.



Figure 22: +1 OAM height.

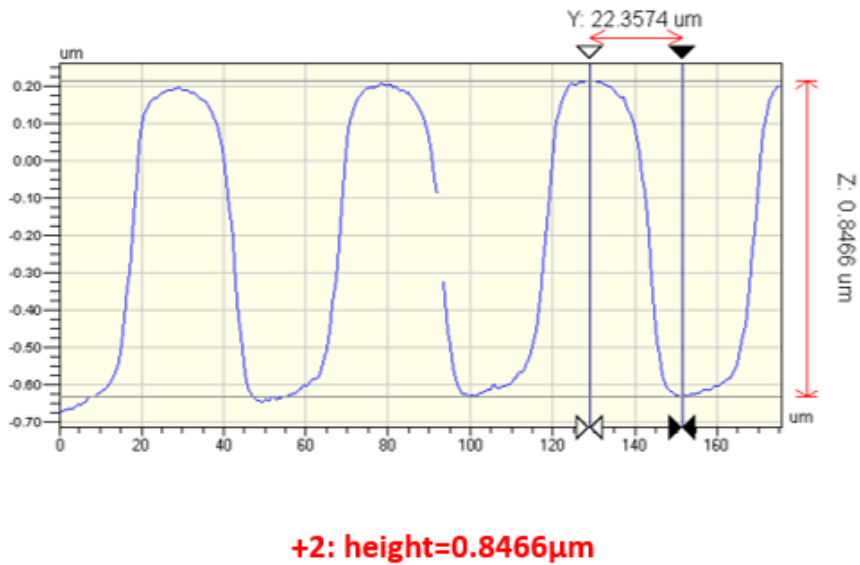
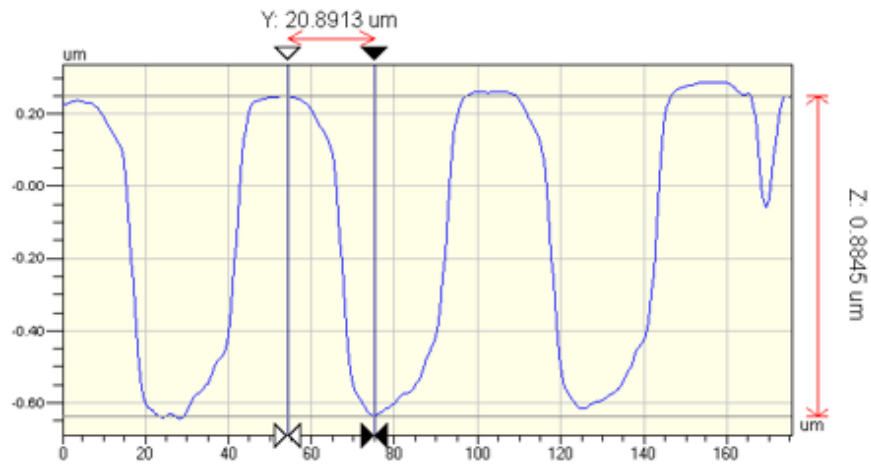


Figure 23: +2 OAM height.



**+3: height=0.8845 $\mu$ m**

Figure 24: +3 OAM height.

This height measurement is only the step height measurement taken at preset reference point on the SPP. This height data does not take into account the full profile of the phase needed to properly observe any type of fabrication error. This allows the possibility of repeatability, as the fabrication height error falls in the range of  $\pm 5\%$  error. The Veeco can also do a surface profile scan for the different OAM modes, Fig. 25 and 26 show a 3D layout for a +2 and +3 OAM profile, although this is a small sample of the actual SPP.

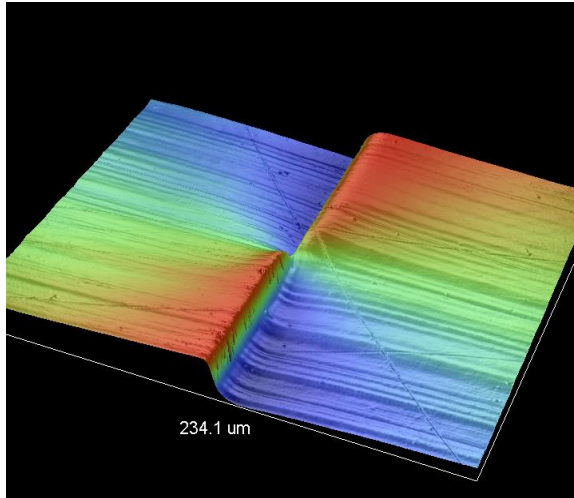


Figure 25: 3D profile of +2 mode.

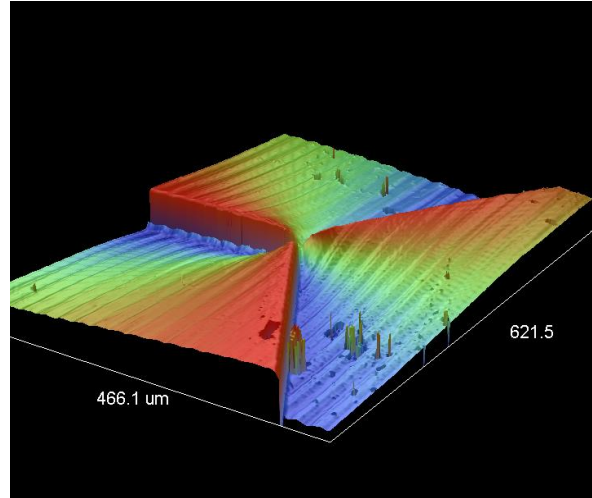


Figure 26: 3D profile of +3 mode.

After fabrication the outputs of the beam are tested to ensure a donut like intensity is obtained and also to see how much beam intensity is lost. Table 1 shows the intensity in percentage of the beam after it goes through the fabricated SPP. The material and behavior of the SPP decreases the power of the input beam which could cause problems later on.

Table 1: Output beam intensity.

Charge	Intensity (%)
1	76.03576
2	74.26659
3	46.735

## 7. Simulation Evaluation of Crosstalk

In order to observe how the fabricated SPPs will affect crosstalk, an ideal MZ demultiplexer are mathematically modelled and implemented by Matlab.

The simulation code is a segmented interferometer. The code takes any matrix and averages it down to a 100 by 100 matrix that is assigned to a detector plane which is sampled according to Eq. 13 and 14 for each LG mode where  $\Delta$  is pixel pitch and  $100\Delta$  is the physical size of the sample. For the analysis,  $\Delta=40$  um is used, which corresponds to the area of interest of 4x4mm. The matrix goes into the interferometer that splits the matrix into two separate outputs to represent each arm after the first beamsplitter. The two arms go through the respective phase shifts and are added together in the respective port output. The intensity of each output is evaluated for each port in Eq. 15 and 16.

$$LG_1(i,j) = LG_1 \left( \left( -50 + \left( (i-1) + \frac{1}{2} \right) \Delta \right), \left( -50 + \left( (j-1) + \frac{1}{2} \right) \Delta \right) \right) \times \sum_{i,j=1}^{100} \delta \left\{ \left( -50 + \left( (i-1) + \frac{1}{2} \right) \Delta \right), \left( -50 + \left( (j-1) + \frac{1}{2} \right) \Delta \right) \right\} \quad (13)$$

$$LG_2(i,j) = LG_2 \left( \left( -50 + \left( (i-1) + \frac{1}{2} \right) \Delta \right), \left( -50 + \left( (j-1) + \frac{1}{2} \right) \Delta \right) \right) \times \sum_{i,j=1}^{100} \delta \left\{ \left( -50 + \left( (i-1) + \frac{1}{2} \right) \Delta \right), \left( -50 + \left( (j-1) + \frac{1}{2} \right) \Delta \right) \right\} \quad (14)$$

$$P1 = \sum_{i,j} \left| \left( \frac{LG_1+LG_2}{2} \right)^T + \left( \frac{LG_1+LG_2}{2} \right) e^{j\pi} \right|^2 \quad (15)$$

$$P2 = \sum_{i,j} \left| \left( \frac{LG_1+LG_2}{2} \right)^T + \left( \frac{LG_1+LG_2}{2} \right) e^{j0} \right|^2 \quad (16)$$

To ensure the code is appropriately implemented the MZ model will be tested with a perfect plane wave to ensure perfect contrast, which will be represented as a sinusoidal behavior. A plane wave made from a 100 by 100 matrix is sent through the MZ simulation and the contrast is shown in Fig. 27.

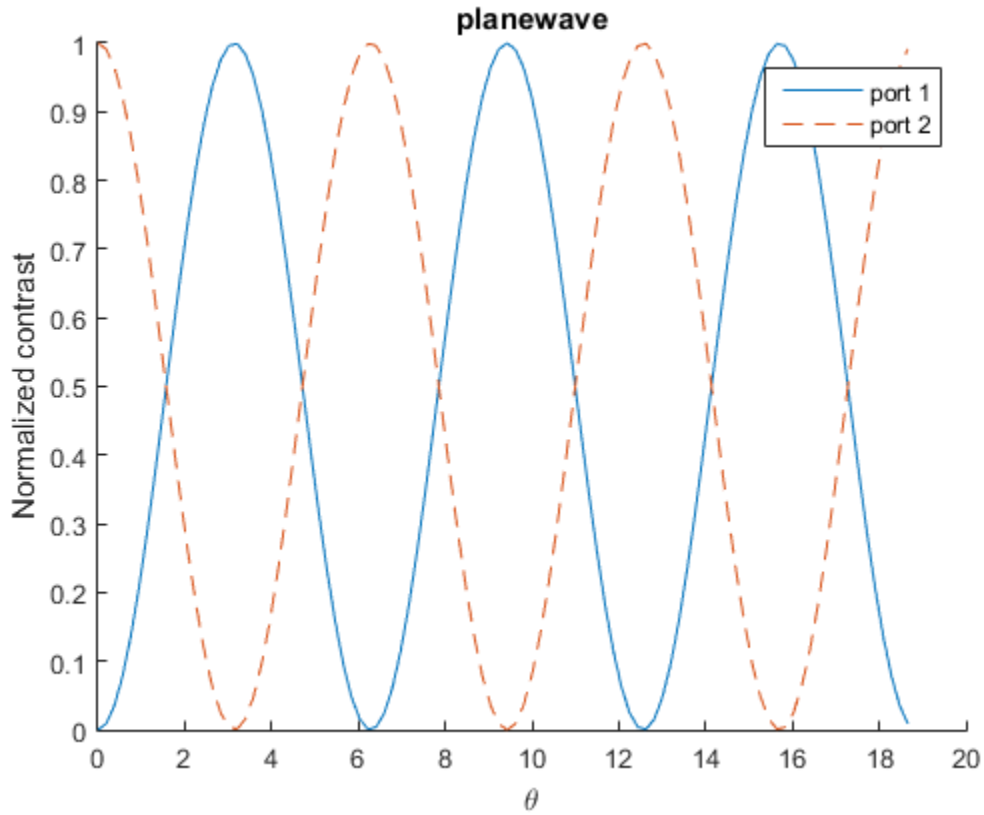


Figure 27: Simulated output from port 1 and 2 as a function of phase difference between two arms of ideal plane wave sent through the MZ simulator.

Next test will be sending two perfect OAM modes of +1 and +2 multiplexed together. The expected output would be a perfect contrast MZ to show the modes are properly separated. Fig. 28 shows the output from the MZ simulator.

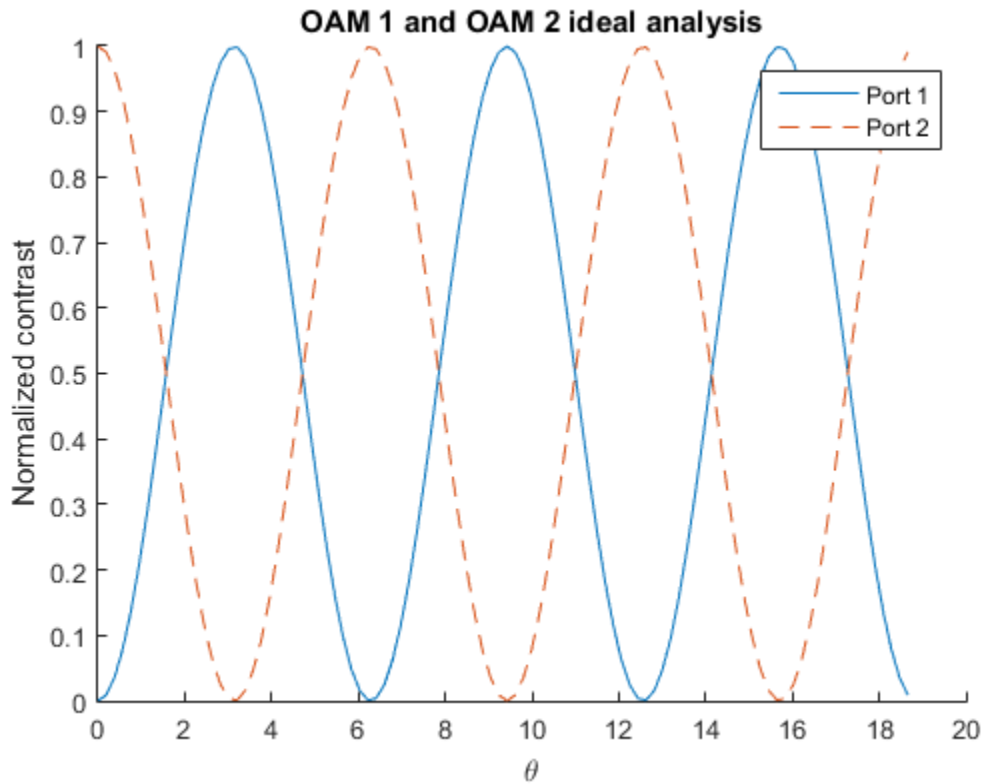


Figure 28: Simulated output from port 1 and 2 as a function of phase difference between two arms of MZ. Ideal OAMs sent through the MZ simulator.

For the final test it would be to observe how the fabricated profiles behave in the MZ, theoretically there will not be a perfect sinusoid because of unavoidable fabrication errors. Taking the fabricated SPPs and obtaining the surface data using Veeco interferometer, a phase is applied to the SPPs and the measured fabricated OAMs are obtained. Fig. 29 shows the contrast of the measured profiles, and as seen the sinusoid is not perfect. Which shows that some of the signal is leaking into the other port preventing it from going to zero and causing it to never reach a one contrast.

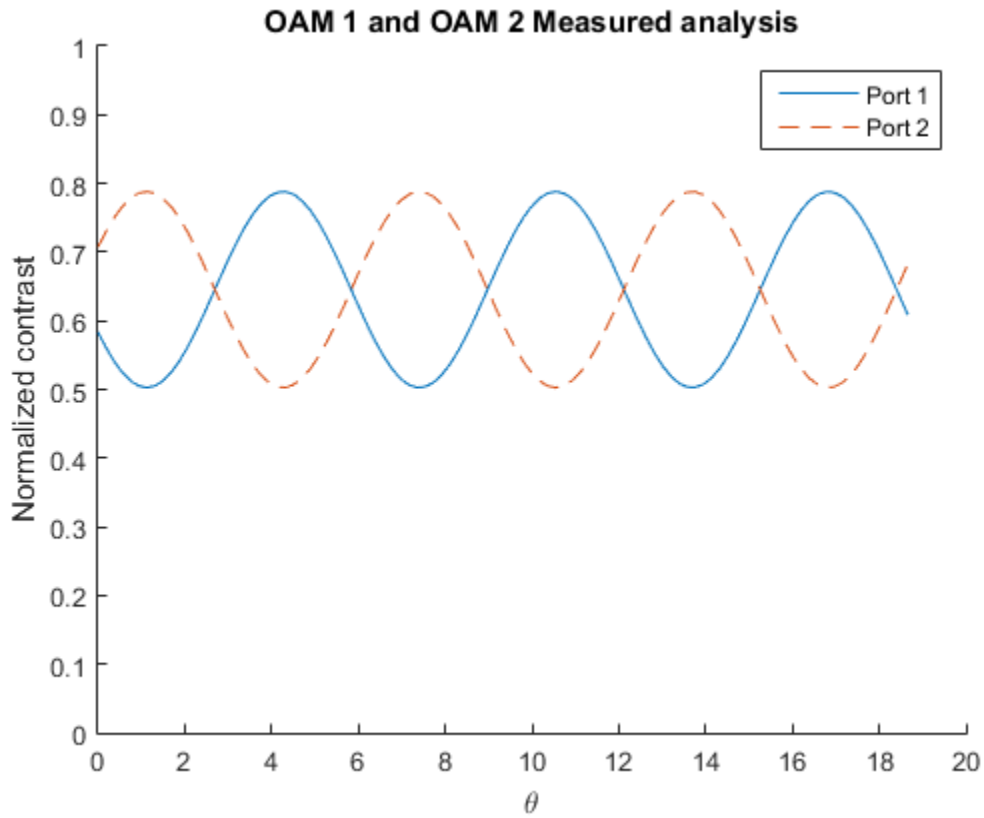


Figure 29: Simulated output from port 1 and 2 as a function of phase difference between two arms of MZ. Measured OAMs sent through MZ simulator.

The fabricated components are showing a lot of contrast issues while going through a perfect MZ. This is not taking into account the intensity loss through the substrate seen in Table 1 and none of the MZ losses themselves.

## 8. Effects of Defects and Height Error for Experimental Crosstalk

Seeing that the fabricated SPPs are creating heavy crosstalk the profiles should be looked at and compared to ideal profiles. Using an interferometer the phase profile of a sample area of 4mm by 4mm can be acquired to be compared to the ideal profile. OAM +1 measured and ideal profile are compared side by side in Fig. 30 and the differences are shown in Fig. 31. OAM +2 measured and ideal profile are compared in Fig. 32 and the difference is seen in Fig. 33. The phase profile is mapped from  $-\pi$  to  $\pi$ .

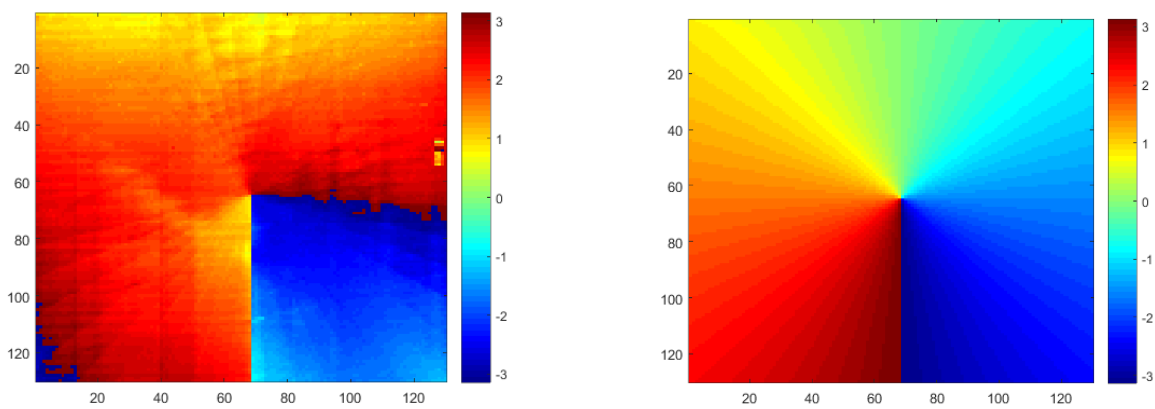


Figure 30: OAM +1 measured and ideal compared side by side.

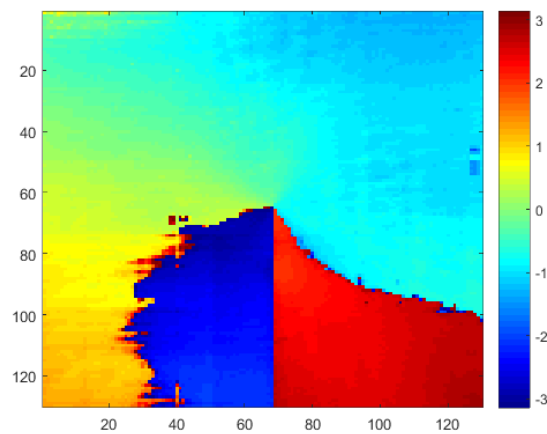


Figure 31: OAM +1 difference.

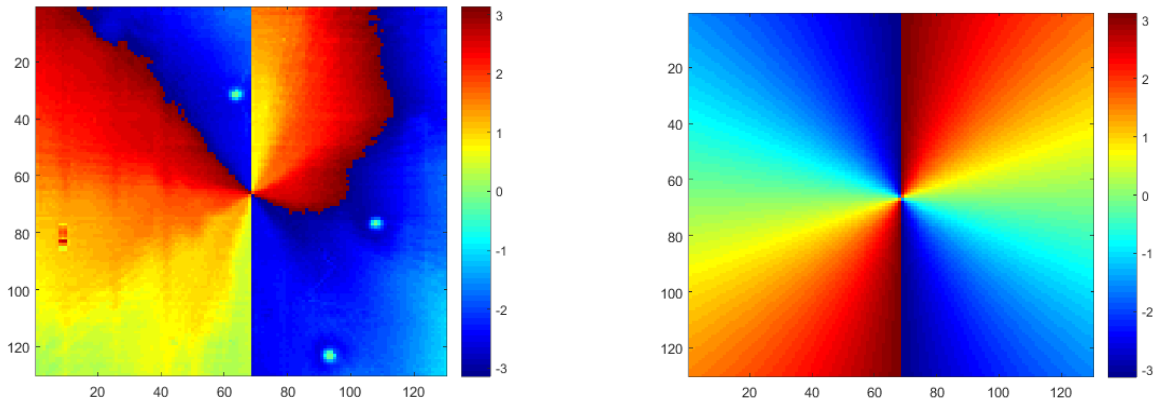


Figure 32: OAM +2 measured and ideal compared side by side.

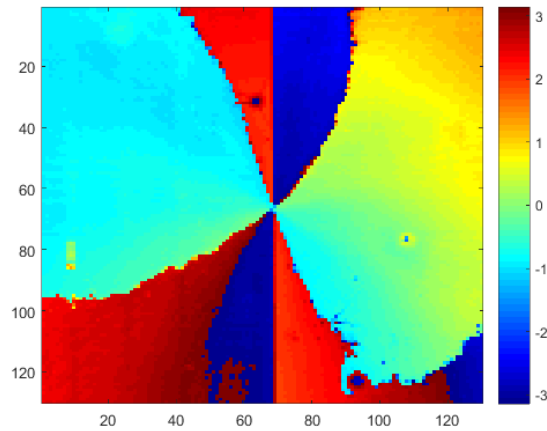


Figure 33: OAM +2 difference.

There was damage and fabrication issues with the SPPs, the damage could have happened overtime, and the fabrication error could make a huge impact. It has been shown that slightly messing with the phase profile can have a huge corruption of the output as seen in the OAM +3 error in Fig. 19, but in this case the phase error is far greater. Which demonstrates the heavy amount of crosstalk in Fig. 29.

This simulation can be used for the physical crosstalk evaluation through the actual system. In the actual experiment the beam itself is tested through the MZ in each port separately with the data shown in Fig. 34.

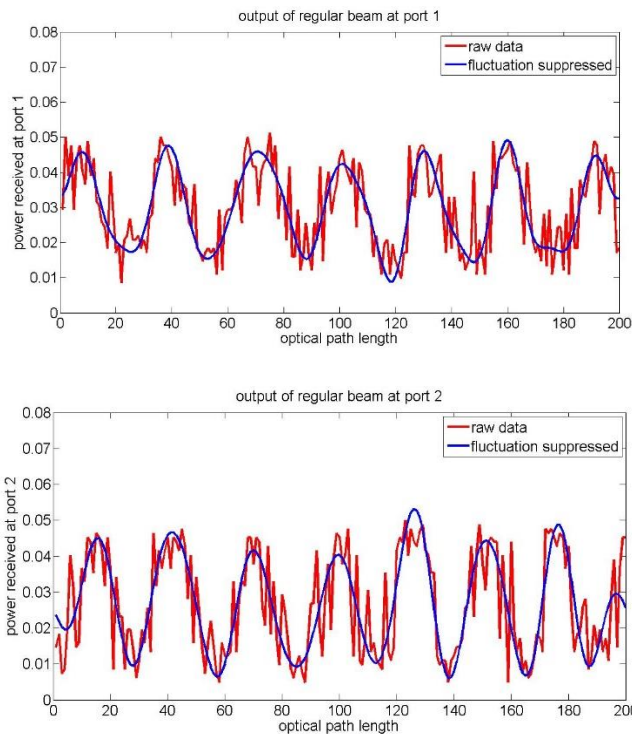


Figure 34: Regular beam output seen at each port of actual MZ

In the regular beam output there is already a substantial loss in power of the original beam and strong fluctuations. These fluctuations are caused by the instability of the MZ, thus a low pass filter was used to filter out the high frequency components. In the graphs of the data the peaks indicate maximum power that is available for one mode at a single port. The valleys should be zero, but there is residual power from the other arm which leads to crosstalk in the initial MZ system. This could be caused by imperfect polarization or beam splitters or any component in the MZ. Next in experimental testing is the OAM

modes separate from each other through the MZ. Fig. 35 is the data of OAM +1 mode by itself and Fig. 36 is the data of the OAM +2 mode by itself.

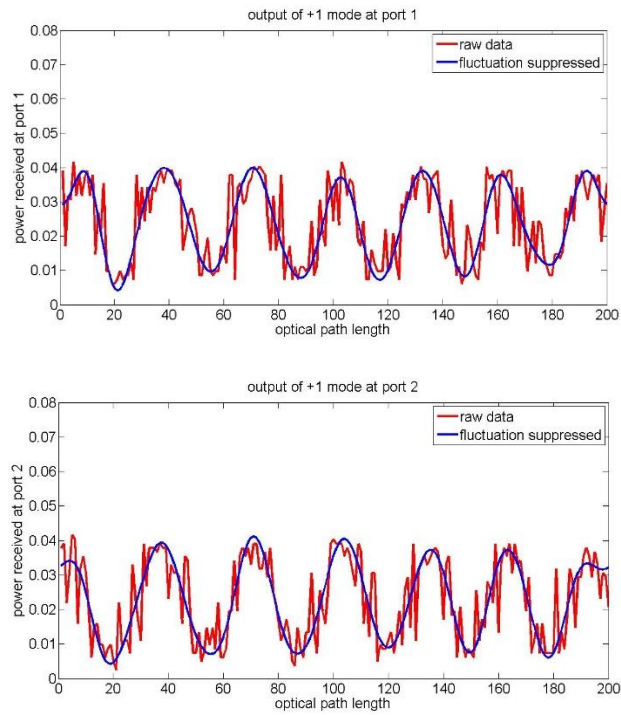


Figure 35: OAM +1 data

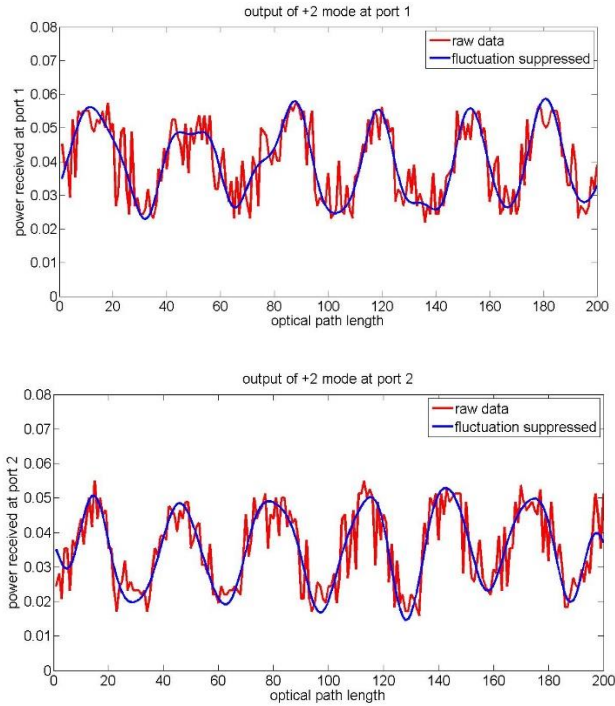


Figure 36: OAM +2 data by itself

By analyzing the separate modes the residual power can be analyzed for different cases if need be. So next if two modes are sent through the MZ, like 0 and +1 mode, in a real detection scenario for port 2 then the peak power for mode 0 should be the valley power for mode +1. In an ideal case of port 2 evaluation for a 0 and +1 mode signal the output from the +1 should have no power leak from mode 0, but according to Fig. 37 this is not the case. This shows that there is crosstalk, therefore examining these graphs can give a lot of information about the crosstalk. This also shows a degradation of modulation in the system. The final evaluation comes in the form of sending +1 and +2 modes together and looking at the output. The data for the +1 and +2 evaluation can be seen in Fig. 38.

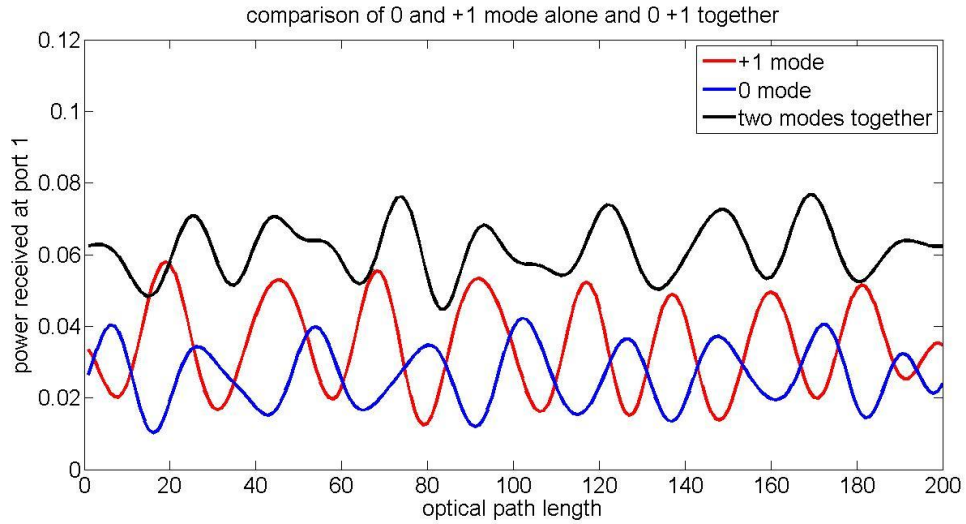


Figure 37: Output of 0 and +1

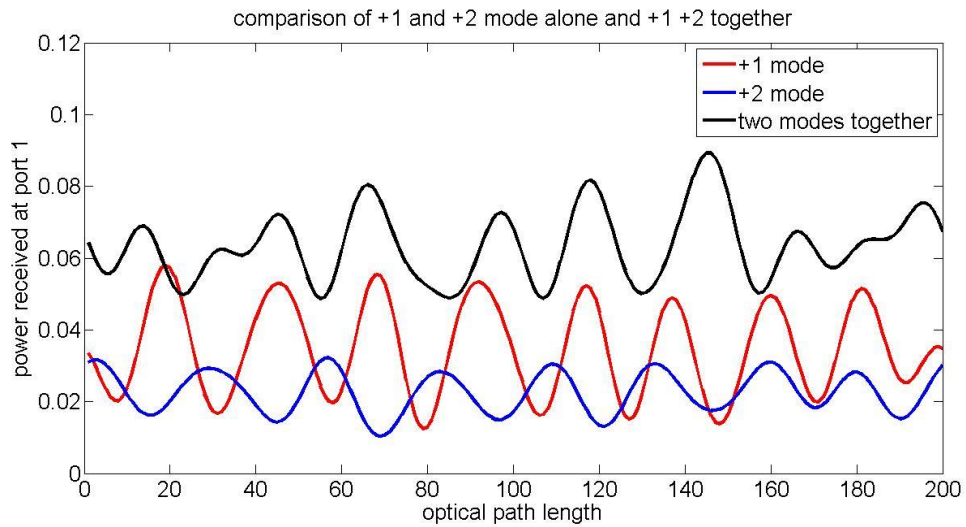


Figure 38: Output of +1 and +2

With the data of the two modes together, from Fig. 38, the output of +1 should be the peak and +2 should be the valley. If the MZ is not leaking any power than the sum of the two modes should be a flat constant, but it is observed that the instability prevents that. So looking at the power of +2 leaking into +1 it can be estimate that there can be up -4.86dB of crosstalk.

Experimental results show that the crosstalk behaved as it should according to the simulations, but there was ignoring of other factors. These factors include MZ loss, SPP loss, instability of the MZ, and potential post damage of the SPP after measuring the profile. The signal also shows an unbalanced signal that could come from power differences from either the Tx or Rx. Seeing that the signal itself is at such a low number and the dB of crosstalk is about  $-39\text{dB}$ , which for a small signal of  $0.06\text{ [W]}$  summation there could be an issue with detector noise. Unless the detector is calibrated for one wavelength it should be possible to detect the modes easily.

## 9. Conclusions and Future Work

In the MZ simulation it was assumed that the MZ was perfect and ideal and the ideal OAMs created for testing were also lossless. It has been shown that there is power loss through the SPPs as well as power loss through a typical MZ, but these were not factored into the simulation. Therefore the contrast produced in Figure 24 was through the measured OAMs without any other loss involved. Thus it would make sense that the actual results have a far lower contrast from all the power loss. Also instability was not taken into account into the simulation, but in the actual data the instability caused the summation of the contrast to not be a constant. Some possible improvements could be making a set of SPPs and not just a single sample for each OAM, to not damage the SPPs either, and to tighten the tolerances of fabrication. Another issue is that the test marks are not a representative of the entire phase profile, if there is error near the center of the profile then that will cause huge issues down the line. The MZ can also be better improved to avoid instability issues and avoid power leaking. In the future it would be nice to include a turbulence chamber and test an adaptive optics system. When creating fabricated SPPs it would be better to make multiple samples and ensure the step index has the proper profile. Switching to communications wavelength would also be part of any future work, as this report established the foundations for basic optical design of free-space links.

## 10. Matlab code

SPP and Mode Converter creation and simulation

```
%%  
% Alonzo Espinoza  
% Opti 600D Final  
% Exploring and looking at a mode converter  
%%  
  
clc  
clear all  
  
AU=2.1e-6; % pixel size  
W=1e-3; % size of sample  
  
n=round(W/AU); % samples  
  
l=2; % charge  
  
gamma=0; % arbitrary phase in mode converter  
delta=1; % Mode conversion  
a=1; % Mode converter deformation  
CH=1; % +/- change in phi  
N=1.468; % index of plate  
  
mask=zeros(n); % make proper sized zeros called mask  
maskt=zeros(n); % maskt is the size of the mode converter  
mask2=zeros(n); % Output mask  
  
dlam=1; % change in wavelength  
lam=dlam*532e-9; % Reconstruction wavelength  
f=3e8/lam; % Frequency  
k=2*pi/lam; % wave number  
w=2*pi*f; % angular frequency  
t=0; % Time variable  
z=0; % direction of propagation  
  
l=1:n; % Sizing  
x=l-n/2; % x vector  
y=n/2-l; % y vector  
[X,Y]=meshgrid(x,y); % vector of x,y  
  
phi=atan2(X,Y); % vortex phase  
r=sqrt(x.^2+y.^2); % not needed
```

```

% ignore
% A1=exp(-i.*l.*phi).*exp(i.*k.*X-f.*t);
% t=exp(-i.*(delta.*phi-gamma));
%
% A2=t.*A1;
%
% RA2=fft((A2));
%
% figure
% imagesc(real(RA2))
% colormap(gray)
%

A=exp(-1i.*l.*phi); % vortex input
A1=exp(-1i.*(w.*t-k.*z)).*A; %input wave
t=exp(-1i.*a.*((delta.*(CH.*phi))-gamma)); % Mode converter
% t=phi.*(N-1).*l.*lam./(2*pi); % SPP
t2=(delta.*(CH.*phi)).*a-gamma-k.*X; % ignore
A2=t.*A1; % output

mask=(1/(2*pi)).*mod(angle(A),2*pi); % phase profile of vortex
maskt=(1/(2*pi)).*exp(-1i.*mod((t2),2*pi)); % profile of mode converter
mask2=(1/(2*pi)).*mod(angle(A2),2*pi); % angular profile of output beam

% Plot input wave
figure
imagesc((mask))
colormap(gray)
colorbar

% plot mode converter
% figure
% imagesc(real(maskt))
% colormap(gray)
% colorbar

% plot output wave
figure
imagesc((mask2))
colormap(gray)
colorbar

%% Phase conversion (not mode)

% maskp=zeros(n);
% mask2p=zeros(n);

```

```

%
% Q=-pi/2; % phase conversion
%
% Ap=exp(-1i.*l.*(phi+pi/2)); % vortex input with pi/2 rotation
% A1p=exp(-1i.*(w.*t-k.*z)).*Ap; % input wave after pi/2 rotation
% p=exp(-1i.*(l.*Q-gamma)); % phase converter
% A2p=p.*A1p; % phase output
%
% % phase conversion
% maskp=(1/(2*pi))*mod(angle(Ap),2*pi);
% mask2p=(1/(2*pi))*mod(angle(A2p),2*pi);
%
% % plot phase changed input wave
% figure
% imagesc((maskp))
% colormap(gray)
% colorbar
%
% % plot phase conversion
% figure
% imagesc((mask2p))
% colormap(gray)

%% Guassian Beam

% n=2^10; % samples
%
% l=1; % charge
%
% gamma=0; % arbitrary phase in mode converter
% delta=1; % Mode conversion
% a=1; % Mode converter deformation
% CH=1; % +/- change in phi
%
% mask=zeros(n); % make proper sized zeros called mask
% mask2=zeros(n); % Output mask
%
% dlam=1; % change in wavelength
% lam=dlam*532e-9; % Reconstruction wavelength
% f=3e8/lam; % Frequency
% k=2*pi/lam; % wave number
% w=2*pi*f; % angular frequency
% t=0; % Time variable
% z=0; % direction of propagation
%
% l=1:n; % Sizing
% x=l-n/2; % x vector
% y=n/2-l; % y vector

```

```

% [X,Y]=meshgrid(x,y); % vector of x,y
%
% phi=atan2(X,Y); % vortex phase
% r=sqrt(x.^2+y.^2); % not needed
%
% A1g=exp(-1.*(((X.^2)./(2.*(10).^2))+((Y.^2)./(2.*(10).^2)))).*exp(-1i.*(w.*t-k.*z)).*A; %input wave
% t=exp(-1i.*a.*((delta.*(CH.*phi))-gamma)); % Mode converter
% A2g=t.*A1g; % output
%
% mask2g=(1/(2*pi))*mod(angle(A2g),2*pi); % angular profile of output beam
%
% % plot output wave
% figure
% imagesc((mask2g))
% colormap(gray)
% colorbar

```

#### Matlab Code for Mach-Zehnder simulation

```

clear all
clc
close all

C=0;
AF1=0;
AF2=0;
BF1=0;
BF2=0;

P=1;
Q=1;

%Define parameters
lam0 = 532e-9; %wavelength in m
L = .004; %length of square hologram in m
charge1 = 1; %charge of vortex
charge2 = 2; %charge of vortex

AU = 2.1e-6; %resolution of MLT
Nsamples = round(L/AU); %number of samples across hologram
l=1:Nsamples;
x=l-Nsamples/2;
y=Nsamples/2-l;

ng = 1.5195; %index of glass substrate

```

```

n0 = 1; %index of image space

%define spiral plate
[X,Y] = meshgrid(x,y);
theta1 = atan2(X,Y);
theta2 = atan2(X,Y);
SPP1=exp(-1i.*charge1.*theta1);

OAM1=BlockMean(SPP1,16);
O1=OAM1*P;
SPP11=csvread('SPP1_Veeco');
O1err=P*BlockMean(SPP11,17);

SPP2=exp(-1i.*charge2.*theta2);

OAM2=BlockMean(SPP2,16);
O2=OAM2*Q;
SPP22=csvread('SPP2_Veeco');
O2err=Q*BlockMean(SPP22,17);

r=rand(10,10);
% A=O1; %OAM 1 analysis
A=(O1err+O2err)/sqrt(2); % combined analysis
% B=O2; %OAM 2 analysis
B=(O1+O2)/sqrt(2); %combined analysis

NORM1=size(A,1)*size(A,2);
NORM2=size(B,1)*size(B,2);

%OAM 1

A1=A./sqrt(2);
A2=(A./sqrt(2)).*exp(1i*pi/2);
A1R=(A1);
A2R=rot90(A2);
A22=(A2R./sqrt(2)).*exp(1i*pi/2);
A21=(A2R./sqrt(2));

for o=1:100
    phi=(o-1)*6*pi/100;
    for m = 1:numel(A)

        A11=(A1R./sqrt(2)).*exp(1i*phi);
        A12=(A1R./sqrt(2)).*exp(1i*phi).*exp(1i*pi/2);

        %port 1
        AF1 = AF1+(A11(m)+A22(m))*(conj(A11(m))+conj(A22(m)));
        AT1(o)=AF1./(NORM1);
    end
end

```

```

%port 2
AF2 = AF2+(A12(m)+A21(m))*(conj(A12(m))+conj(A21(m)));
AT2(o)=AF2./(NORM1);
end
AF1=0;
AF2=0;
end

%OAM 2

B1=B./sqrt(2);
B2=(B./sqrt(2)).*exp(1i*pi/2);
B1R=(B1);
B2R=(B2);
B22=(B2R./sqrt(2)).*exp(1i*pi/2);
B21=(B2R./sqrt(2));

for o2=1:100
    phi2=(o2-1)*6*pi/100;
for m2 = 1:numel(B)

    B11=(B1R./sqrt(2)).*exp(1i*phi2);
    B12=(B1R./sqrt(2)).*exp(1i*phi2).*exp(1i*pi/2);

    %port 1
    BF1 = BF1+(B11(m2)+B22(m2))*(conj(B11(m2))+conj(B22(m2)));
    BT1(o2)=BF1./NORM2;

    %port 2
    BF2 = BF2+(B12(m2)+B21(m2))*(conj(B12(m2))+conj(B21(m2)));
    BT2(o2)=BF2./NORM2;
end
BF1=0;
BF2=0;
end

figure
hold on
title('OAM 1 and OAM 2 Measured analysis');
ylim([0 1])
%OAM1 port 1
plot(AT1,'-');
%OAM 1 port 2
plot(AT2,'-');
% %sum
% plot(AT1+AT2);

```

```

legend('Port 1','Port 2');

figure
hold on
title('OAM 1 and OAM 2 ideal analysis')
ylim([0 1])
%OAM 2 port 1
plot(BT1,'-');
%OAM 2 port 2
plot(BT2,'--');
legend('Port 1','Port 2');
% %sum
% plot(BT1+BT2);
% legend('Port 1','Port 2','sum');

```

#### Matlab Code for Ideal profile vs measured for SPP1

```

clc
clear all
close all

% need to blockmean the matrices to somewhat similar sizes
% 14 for SPP1, 12 for SPP2V (veeco SPP2)

% next I need to align the matrices centers
% matrix(:,[m])=[] will adjust the X values
% matrix([n],:)=[] will adjust the Y values

% determine m and n by matrix centers

%% Create Ideal SPP2

%Define parameters
lam0 = 532e-9; %wavelength in m
L = .004; %length of square hologram in m
charge1 = 1; %charge of vortex
charge2 = 2; %charge of vortex

AU = 2.1e-6; %resolution of MLT
Nsamples = round(L/AU); %number of samples across hologram
I=1:Nsamples;
x=I-Nsamples/2;
y=Nsamples/2-I;

ng = 1.5195; %index of glass substrate
n0 = 1; %index of image space

```

```

%define spiral plate
[X,Y] = meshgrid(x,y);
theta1 = atan2(X,Y);
theta2 = atan2(X,Y);
SPP2=rot90(exp(-1i.*charge2.*theta1));

%% Read in measured Veeco SPP1

filename='SPP2_Veeco';
SPP2V=(csvread(filename));

%% Plot them to find centers

figure;imagesc(angle(SPP2));colormap(jet);colorbar

figure;imagesc(angle(SPP2V));colormap(jet);colorbar

%% blockmean

close all

O2a=BlockMean(SPP2,14);

O2b=BlockMean(SPP2V, 12);

%% plot blockmean to find true centers

figure;imagesc(angle(O2a));colormap(jet);colorbar
figure;imagesc(angle(O2b));colormap(jet);colorbar

% O2a take away 2 from the Y axis, O2b take away 5 from X axis

%% removal of the matrix stuff

for m=1:2
    O2a([m],:)=[];
end

for n=1:5
    O2b(:,[n])=[];
end

figure;imagesc(angle(O2a));colormap(jet);colorbar
figure;imagesc(angle(O2b));colormap(jet);colorbar

%% Crop to equal matrix

O2aa=O2a(1:130,1:130);
O2bb=O2b(1:130,1:130);

close all

```

```

figure;imagesc(angle(O2aa));colormap(jet);colorbar
figure;imagesc(angle(O2bb));colormap(jet);colorbar

O2T = O2aa-O2bb;
figure;imagesc(angle(O2T));colormap(jet);colorbar

%% RMS

% E2D=rms(O2T,2);
% figure;plot(E2D);

% E3D=rms(O2T,3);
% figure;imagesc(E3D);colormap(jet);colorbar

```

### Matlab Code for Ideal profile vs measured for SPP2

```

clc
clear all
close all

% need to blockmean the matrices to somewhat similar sizes
% 14 for SPP1, 12 for SPP2V (veeco SPP2)

% next I need to align the matrices centers
% matrix(:,[m])=[] will adjust the X values
% matrix([n],:)=[] will adjust the Y values

% determine m and n by matrix centers

%% Create Ideal SPP2

%Define parameters
lam0 = 532e-9; %wavelength in m
L = .004; %length of square hologram in m
charge1 = 1; %charge of vortex
charge2 = 2; %charge of vortex

AU = 2.1e-6; %resolution of MLT
Nsamples = round(L/AU); %number of samples across hologram
I=1:Nsamples;
x=I-Nsamples/2;
y=Nsamples/2-I;

ng = 1.5195; %index of glass substrate
n0 = 1; %index of image space

%define spiral plate
[X,Y] = meshgrid(x,y);
theta1 = atan2(X,Y);

```

```

theta2 = atan2(X,Y);
SPP2=rot90(exp(-1i.*charge2.*theta1));

%% Read in measured Veeco SPP1

filename='SPP2_Veeco';
SPP2V=(csvread(filename));

%% Plot them to find centers

figure;imagesc(angle(SPP2));colormap(jet);colorbar

figure;imagesc(angle(SPP2V));colormap(jet);colorbar

%% blockmean

close all

O2a=BlockMean(SPP2,14);

O2b=BlockMean(SPP2V, 12);

%% plot blockmean to find true centers

figure;imagesc(angle(O2a));colormap(jet);colorbar
figure;imagesc(angle(O2b));colormap(jet);colorbar

% O2a take away 2 from the Y axis, O2b take away 5 from X axis

%% removal of the matrix stuff

for m=1:2
    O2a([m],:)=[];
end

for n=1:5
    O2b(:,[n])=[];
end

figure;imagesc(angle(O2a));colormap(jet);colorbar
figure;imagesc(angle(O2b));colormap(jet);colorbar

%% Crop to equal matrix

O2aa=O2a(1:130,1:130);
O2bb=O2b(1:130,1:130);

close all

figure;imagesc(angle(O2aa));colormap(jet);colorbar
figure;imagesc(angle(O2bb));colormap(jet);colorbar

O2T = O2aa-O2bb;

```

```
figure;imagesc(angle(O2T));colormap(jet);colorbar

%% RMS

% E2D=rms(O2T,2);
% figure;plot(E2D);

% E3D=rms(O2T,3);
% figure;imagesc(E3D);colormap(jet);colorbar
```

## 11. References

- [1] Ming Li, Yuzuru Takashima, Xiaole Sun, Zhongyuan Yu, Milorad Cvijetic, “Enhancement of channel capacity of OAM-based FSO link by correction of distorted wave-front under strong turbulence”, *Opt. Express* 22, 31337-31346.
- [2] L. Allen, M. W. Beijersbergen, R.J. C. Spreeuw, and J. P. Woerdman, “Orbital angular momentum of light and the transformation of Laguerre-Gaussian laser modes”, *Phys. Rev. A* 45, 8185.
- [3] Ivan P. Kaminow, Tingye Li and Alan E. Willner, *Optical Fiber Telecommunications VIB: Systems and Networks, Sixth Edition*
- [4] Paul Fulda, *Precision Interferometry in a New Shape: Higher-order Laguerre-Gauss Modes for Gravitational Wave Detection*
- [5] OptiScan by Tom Milster Group from [http://fp.optics.arizona.edu/milster/optiscan/OptiScan\\_MENU\\_PAGE.htm](http://fp.optics.arizona.edu/milster/optiscan/OptiScan_MENU_PAGE.htm)
- [6] J. Arlt , K. Dholakia , L. Allen & M. J. Padgett, “The production of multiringed Laguerre–Gaussian modes by computer-generated holograms”, *Journal of Modern Optics* Vol. 45, Iss. 6.
- [7] M.W. Beijersbergen, R.P.C. Coerwinkel, M. Kristensen, J.P. Woerdman, “Helical-wavefront laser beams produced with a spiral phaseplate”, *Optics Communications*, Volume 112, Issues 5–6.
- [8] Gregorius C.G. Berkhout, Martin P.J. Lavery, Johannes Courtial, Marco W. Beijersbergen, and Miles J. Padgett, “Efficient sorting of orbital angular momentum states of light”, *Opt. Express* 20, 24444-24449.
- [9] Jonathan Leach, Miles J. Padgett, Stephen M. Barnett, Sonja Franke-Arnold, and Johannes Courtial, “Measuring the Orbital Angular Momentum of a Single Photon”, *Phys. Rev. Lett.* 88, 257901.
- [10] Chris Summitt, Sunglin Wang, Lee Johnson, Melissa Zaverton Tao Ge, Tom Milster, and Yuzuru Takashim, “Micro-optics fabrication by mask-based and mask-less mixed lithography process towards 3D optical circuits”, *Proc. SPIE 8974, Advanced Fabrication Technologies for Micro/Nano Optics and Photonics VII*, 89740C.
- [11] M. Zaverton, J. Sierchio, Y. S. Kim, D. Hansen, W. Bletcher, J. Tamkin, T. D. Milster, “Maskless Lithography Tool for Fabrication and Inspection of Diffractive Optical Elements and Computer Generated Holograms”, *International Optical Design Conference and Optical Fabrication and Testing* , OSA Technical Digest (CD) (Optical Society of America, 2010), paper OTuC5.

## List of Publications

1. Alonzo Espinoza, Wenbo Gao, Garret Odom, Milorad Cvijetic, Yuzuru Takashima, "Optical design of communication simulator for orbital angular momentum based free-space link with an adaptive optics receiver", Submitted for SPIE 9614, Laser Communication and Propagation through the Atmosphere and Oceans IV, 96140P.
2. Christopher Dumas, Adam Bernstein, Alonzo Espinoza, Donovan Morgan, Kevin Lewis, Matt Nipper, Harrison H. Barrett, Matthew A. Kupinski, Lars R. Furenlid, "SmartCAM: an adaptive clinical SPECT camera", Submitted for SPIE 8853, Medical Applications of Radiation Detectors III, 885307.